VALIDATION OF AN ELECTROMAGNETIC SOLVER USED FOR INVERSE SCATTERING APPLICATIONS

Authors: Simone Genovesi, Silvia Evangelisti
Date: April 2006

Introduction

This report is intended to validate a numerical code proposed in [1] and employed to solve the direct problem in inverse scattering applications [2,3]. The solver is able to calculate the reflection coefficient of a multilayered object under two main hypothesis regarding the incidence field and the structure of the object under investigation. The former hypothesis which needs to be satisfied is that the incidence field has to be a plane wave, while the latter requires the infinite extension of the layered medium along the dimensions orthogonal to the direction of the impinging wave.

First of all, in order to evaluate the reliability of the proposed solver, the reflection coefficients of several multilayered objects have been calculated by using commercial codes (Ansoft HFSS and Designer) [4] and compared with the ones produced by our code. In this case both the two mentioned hypothesis are satisfied and it is possible to investigate the reliability of the code for both the magnitude and phase response.

Then, the results produced by the solver have been also compared with real measurements obtained in two test campaigns. This last analysis is of great importance to better understand the limits of the numerical code when its underlying assumptions cannot be satisfied, as in the case of a real-word environment.

1. Preliminary validation with a multilayered structure.

The first validation has been accomplished by using HFSS. The configuration under analysis is shown in Fig.1. It is composed by 4 different layers of infinite extension on the x-y plane. The assumed incident radiation is a plane wave impinging normally on the top interface between the free space and the layered structure. As said before, infinite extension of the layered medium and normal incidence are the hypotheses upon which our numerical solver is based and then they are also employed in the HFSS simulation.

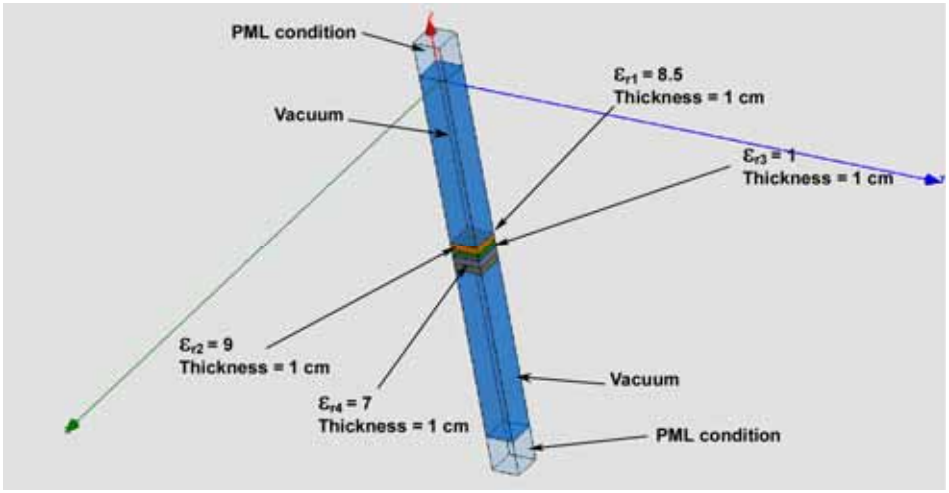

Fig. 1 – Configuration of the simulated structure. The four slabs have the same thickness (1 cm) but different dielectric constants ($\varepsilon_{r1} = 8.5$, $\varepsilon_{r2} = 9$, $\varepsilon_{r3} = 1$, $\varepsilon_{r4} = 7$).

The magnitudes of the reflection coefficient at the interface, calculated by both our solver and HFSS, are shown in Fig.2. The two results agree very well and this proves the reliability of the solver in calculating the amount of power reflected by a multilayered structure.

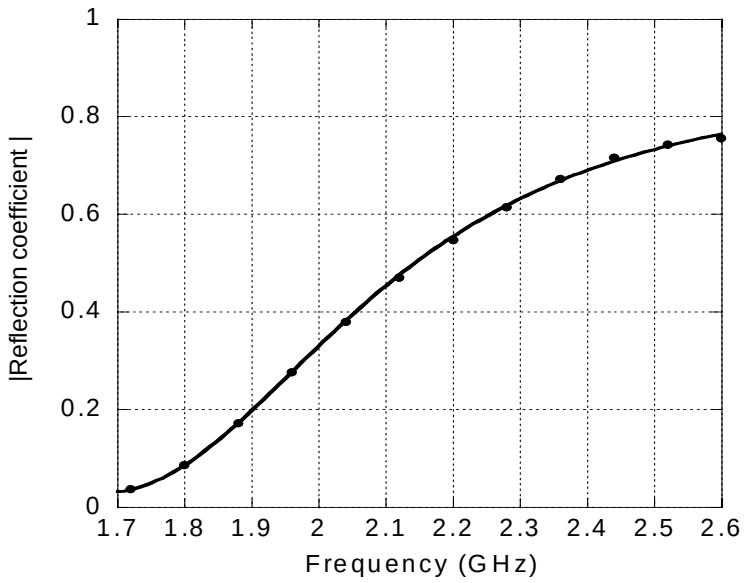

Fig. 2 – Comparison between the reflection coefficients obtained by probing with a plane wave the structure presented in Fig.1. The frequency range is from 1.7 GHz to 2.6 GHz. The incidence of the plane wave is normal. The results obtained by our solver are indicated with the solid line while the dots represent the solution given by Ansoft HFSS.

Another example is given in Fig. 3 where it is possible to compare the results for a plexiglass slab (ε_r= 2.0) with thickness equal to one centimeter.

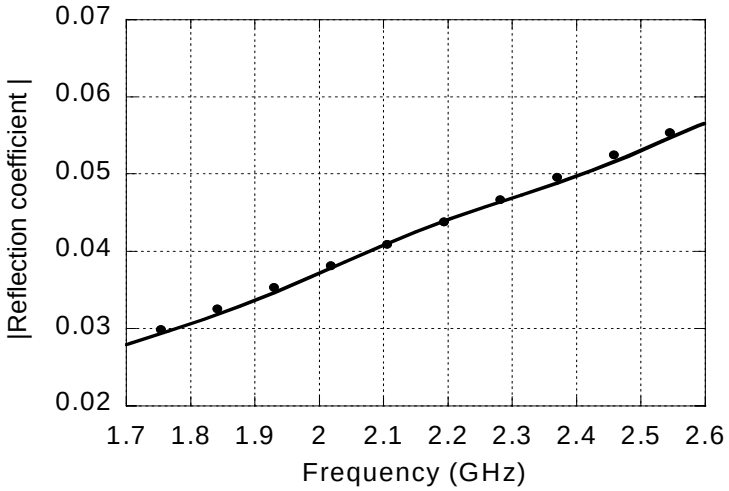

Fig. 3 – Comparison between the power reflected by a single plexiglass brick (ε_r = 2.0), evaluated by our solver (solid line) and by Ansoft HFSS (dots).

In order to validate the analysis of the reflection coefficient phase, we have employed a different code (Ansoft Designer) as a benchmark for our solver. The choice of using another solver for the evaluation of the phase is related to the performance of the numerical methods on which HFSS and Designer are based. The second has proved to be more reliable in evaluating phase responses with an output probe put along an interface since it does not present any numerical instability of the solution respect to the output position. In this case the configuration under analysis is a slab of alumina (ε_r= 8.5), one centimeter thick. Even in this case, the layered medium has an infinite extension on a plane orthogonal to the incidence plane wave. The result is reported in Fig. 4.

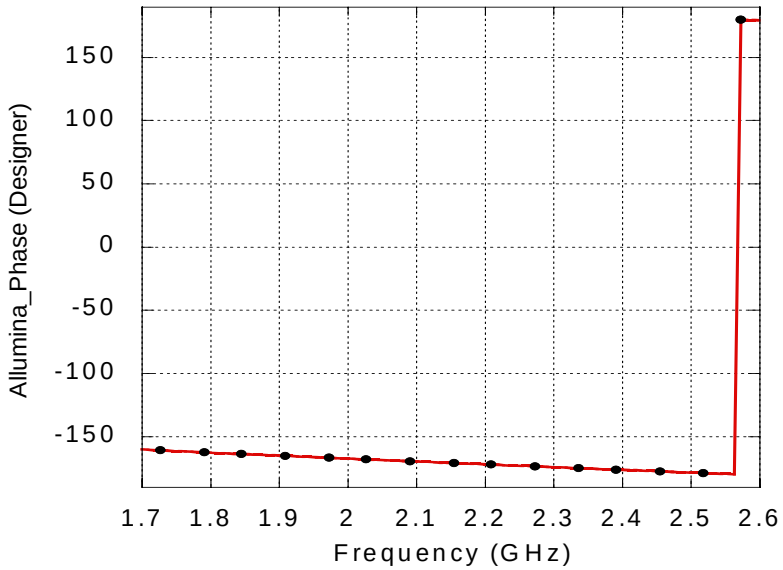

Fig. 4 – Comparison between the phases of the reflection coefficient in the alumina case. The red continuous line is the phase calculated by using the solver, the black dots represent the solution obtained by Designer.

These two comparisons allow us to affirm the reliability of our solver for calculating both the magnitude and the phase of the reflection coefficient of a layered medium tested with a plane wave, since there is a total agreement with the results obtained by using reliable commercial codes.

2. Real measurements (non ideal case).

To test the robustness of our solver when the hypotheses of the normal-incidence plane wave and the infinite extension of the multilayered medium are not satisfied, we have set up a test bed for measurements, as sown in Fig. 5.

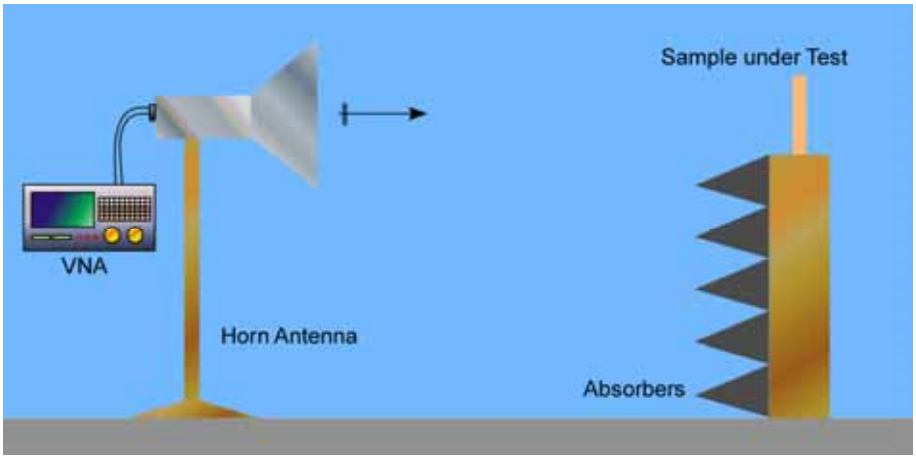

Fig. 5 – Measurements set up for collecting data in a real environment to compare with the simulated results compute by the solver in the ideal case.

The employed Vector Network Analyzer has been an HP 8753b (bandwidth from 300 KHz to 3 GHz, calibration kit N – 50 Ohm, test set T/R HP85044A) while the horn antenna was a WAVETRONICS 6002-00 (bandwidth from 1.7 GHZ to 2.6 GHz). The following Fig. 6-7 show in detail the antenna characteristics while Fig.8-13 present the gain and the electric field calculated with two different commercial solvers, namely HFSS and CST [5].

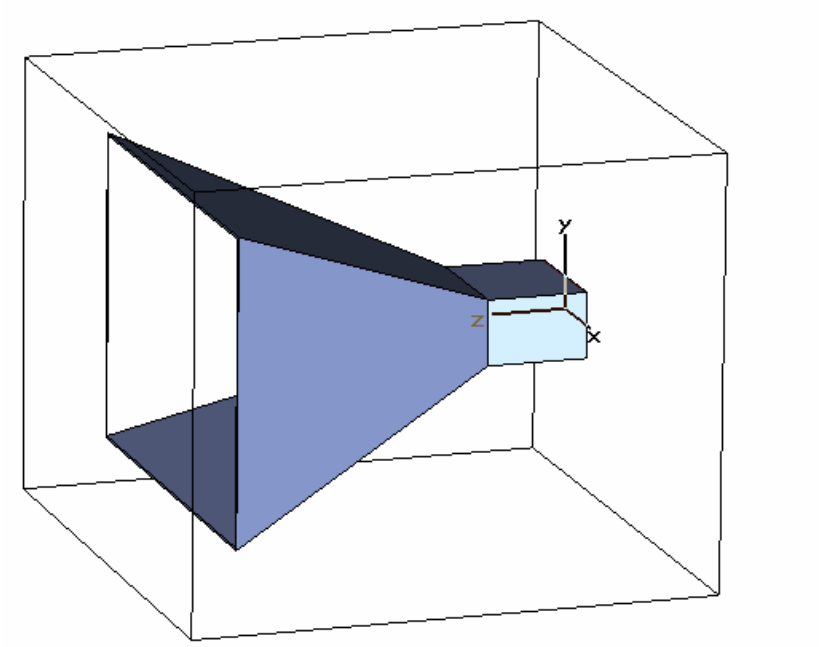

Fig. 6 – Three-dimensional view of the horn antenna used for the measurements.

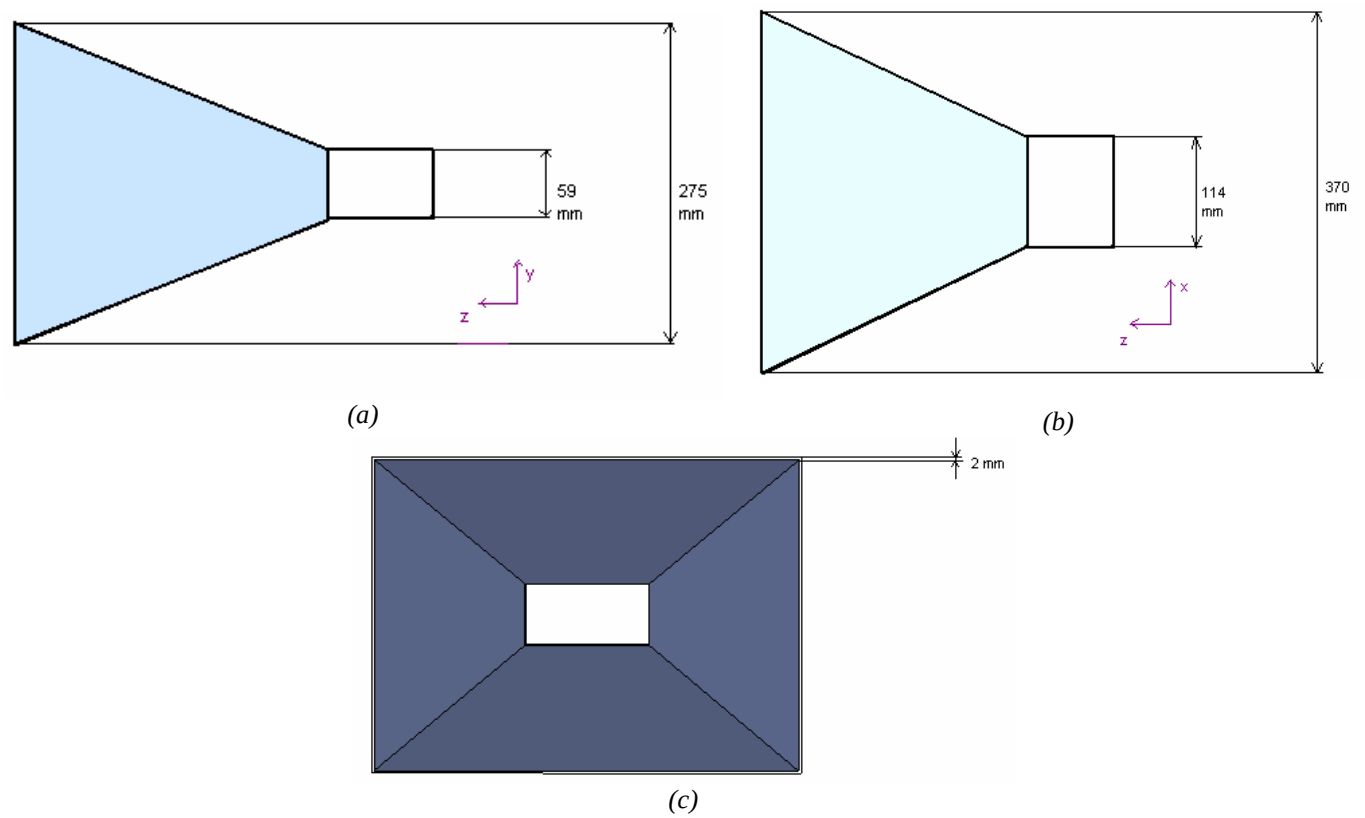

(a) *(b)* *(c)*

Fig. 7 - (a) View on z-y plane; (b) View on z-x plane; (c) View on x-y plane.

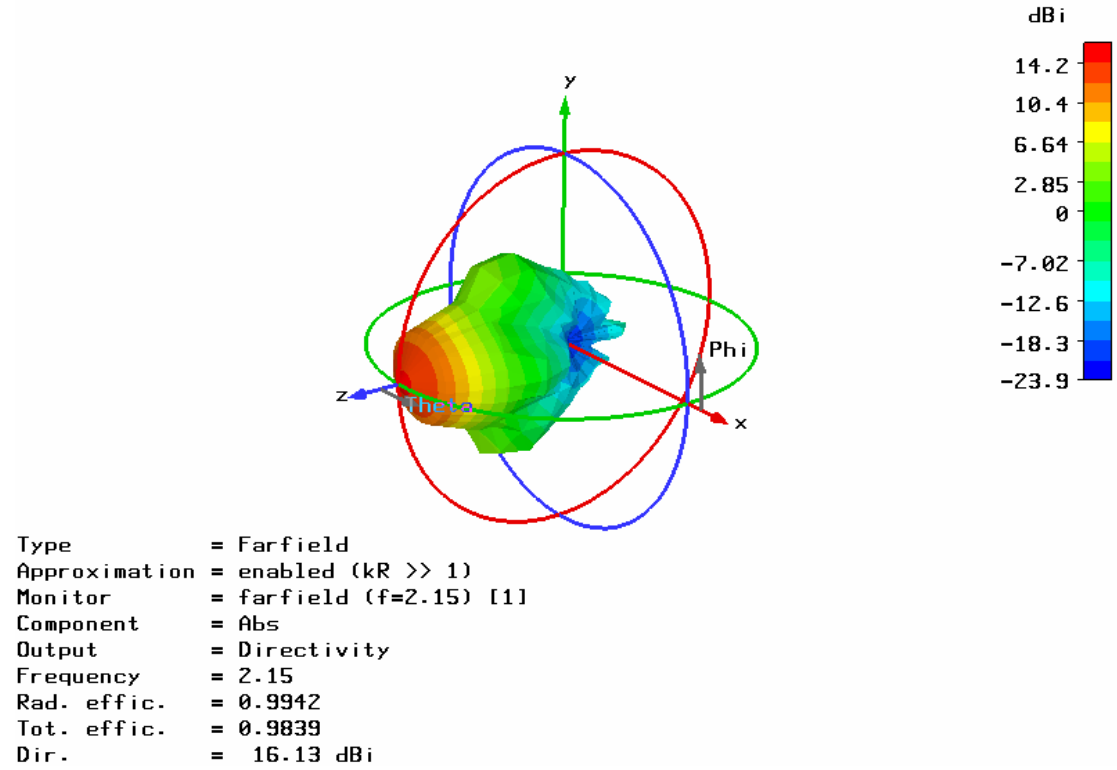

Fig. 8 - Directivity of the horn antenna in free space obtained by using CST: three-dimensional representation.

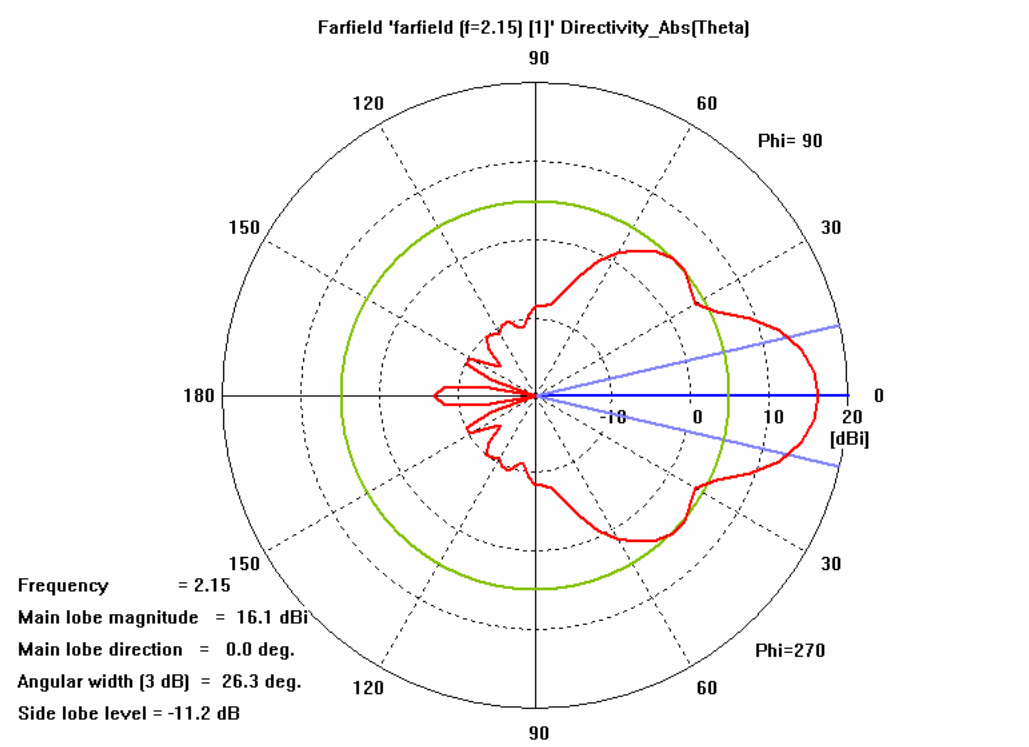

Fig. 9 – Directivity of the horn antenna in free space obtained by using CST: polar representation.

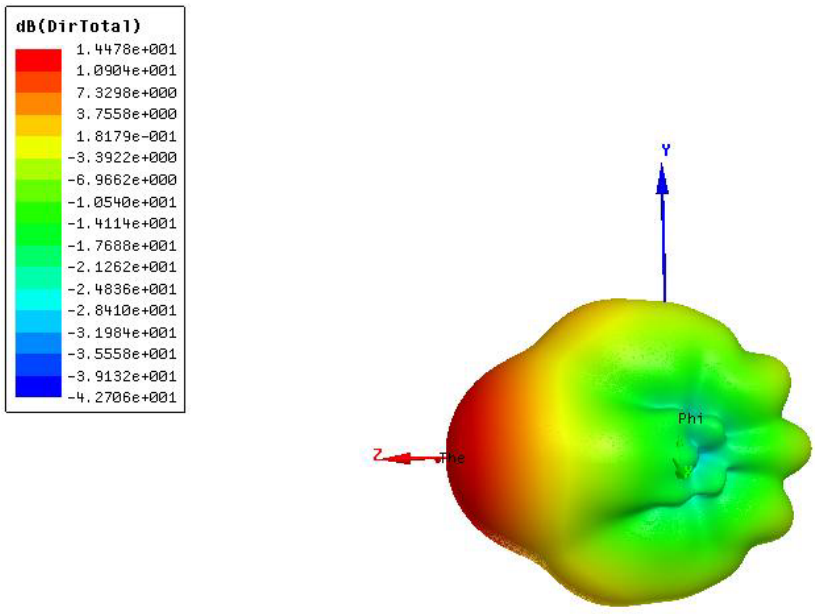

Fig. 10 – Three-dimensional representation of the directivity of the horn antenna in free space obtained by using HFSS.

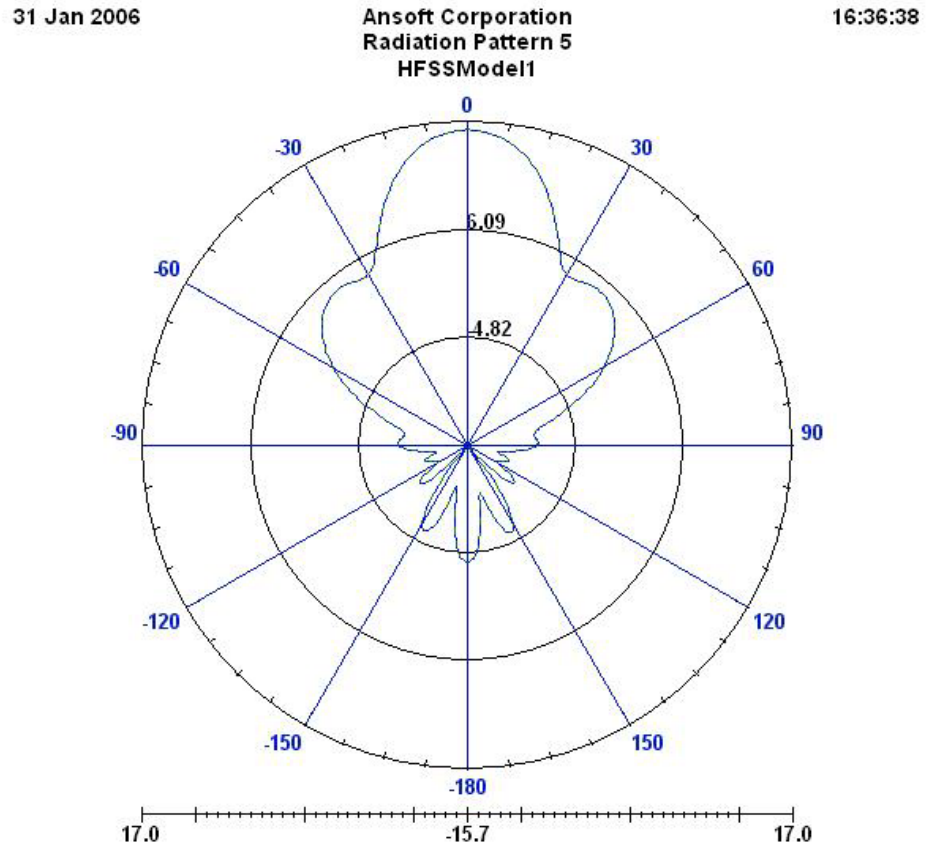

Fig. 11 – Directivity of the horn antenna in free space obtained by using HFSS: polar representation (in the plane phi=90 degrees).

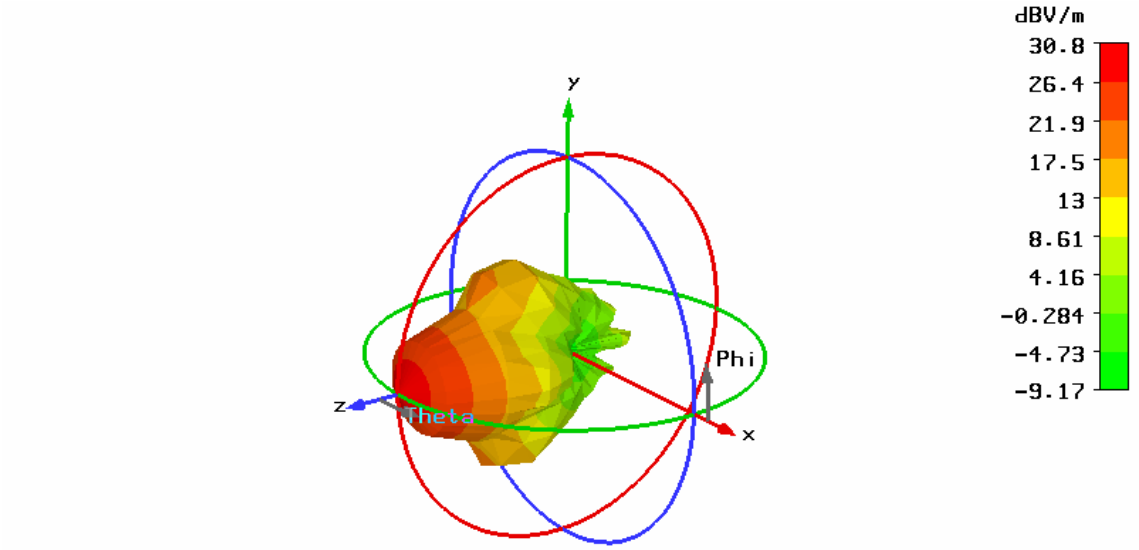


```
Type          = Farfield
Approximation = enabled (kR >> 1)
Monitor       = farfield (f=2.15) [1]
Component     = Abs
Output        = E-Field(r=1m)
Frequency     = 2.15
Rad. effic.   = 0.9942
Tot. effic.   = 0.9839
Emax          =  30.83 dBV/m
```

Fig. 12 – Behavior of the electric field of the horn antenna calculated with CST: three-dimensional representation.

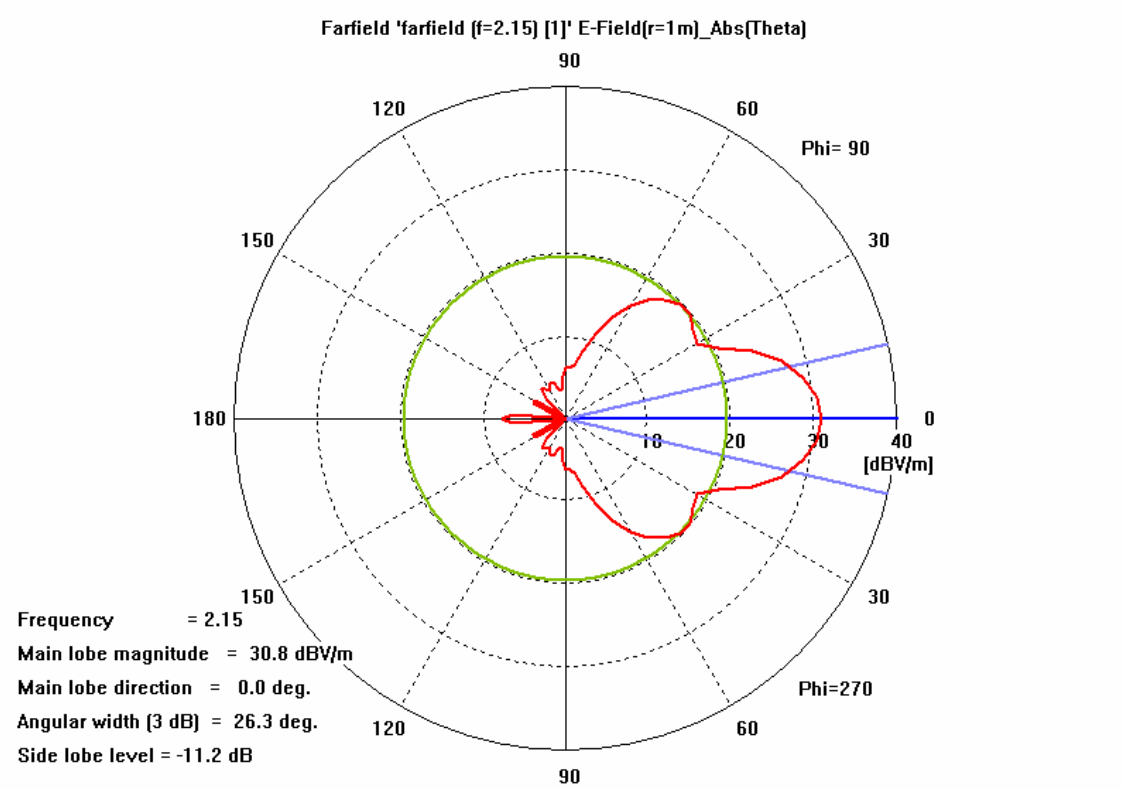

(b)

Fig. 13 – Behavior of the electric field of the horn antenna calculated with CST: polar representation.

It can be seen that the two directivity patterns are quite in good agreement. The shape of the patterns and the HPBW are almost the same while the main lobe magnitude differs around 1.5 dB. A possible reason for this difference could be found on the different type of the sources adopted by the two solvers or in slight differences between the two three-dimensional antenna models. In fact, for the HFSS case, we have necessarily neglected for computational reasons the thickness of the metal and considered the antenna only composed by PEC surfaces.

For the test measurements we have used different configurations of square samples (10cm x 10cm):

- A plexiglass slab (ε_r=2.0) with thickness equal to 1cm;
- An alumina slab (ε_r= 8.5) of the same thickness;
- A three-layer structure composed by a slab of alumina, a slab of plexiglass and another slab of alumina.

After the calibration of the probing system, we have measured the scattering produced by the background environment (without any sample) in order to subtract its contribution to all the other measurements.
Then we have measured the field scattered by a PEC plate of the same size of the other samples, which allow us to have a reference for normalizing the reflected power. In fact, following this procedure, we do not need to know the exact frequency behavior of the gain and the distance between the antenna and the sample to calculate the attenuation in the free space. Thanks to this measure we are able to normalize, for each frequency (201 samples within the range of the horn antenna) , the value of the reflection coefficient and this allows us to compare these results with those given by the solver in the ideal case.

The first campaign comprises only the measurements obtained from a single calibration while the second campaign comprises two set of measurements, each one with its own calibration.

Case #1: Environment

The two average realizations of the reflection coefficient magnitude measured during the second campaign are shown in Fig. 14(a). Each average refers to a different calibration. They are compared with the average of the results of the first campaign in the following Fig. 14(b).

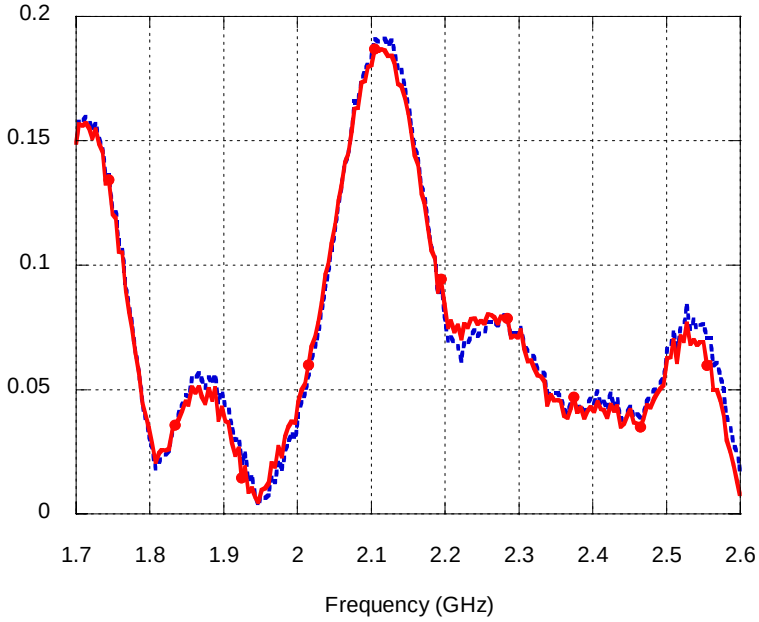

(a)

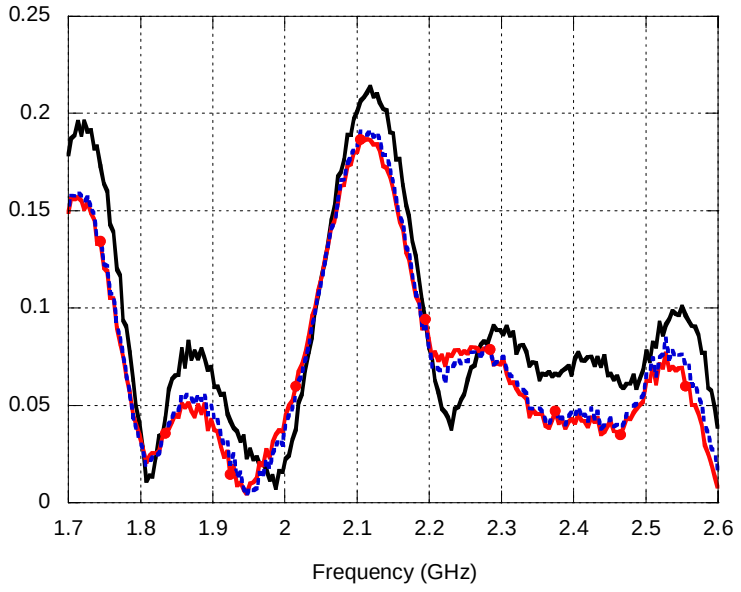

(b)

Fig. 14 – Comparison between the average reflection coefficient magnitude of the first (continuous red line with dots) and second (dashed blue line) calibration of the second campaign; (b) comparison between the average reflection coefficient magnitudes of the first (black) and second (red and blue) campaign.

Case #2: PEC

In Fig. 15, the two average reflection coefficients obtained in the second campaign are shown. The area of the square PEC plate is the same as the one of the other dielectric slabs used in the probing sessions (10cm x 10 cm). The background has been subtracted. In Fig. 15, it is possible to see the phase of the reflection coefficient, which is quite close to 180°/-180° in the frequency range of interest. This fact ensures the correctness of our phase reference.

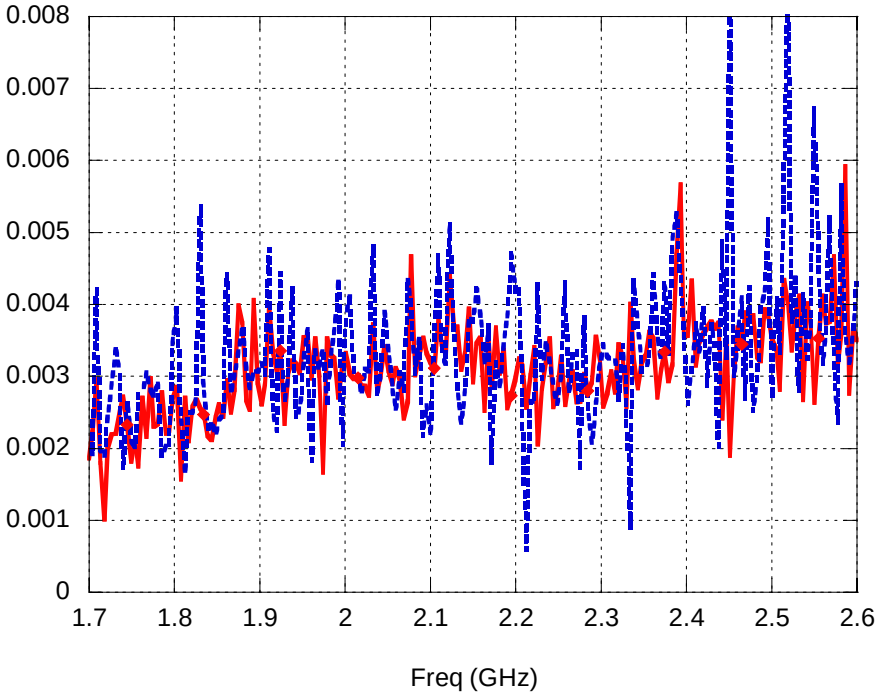

(a)

Fig. 15 – Comparison between the average of the reflection coefficient magnitude for a PEC slab of the first (continuous red line with dots) and second (dashed blue line) calibration of the second campaign.

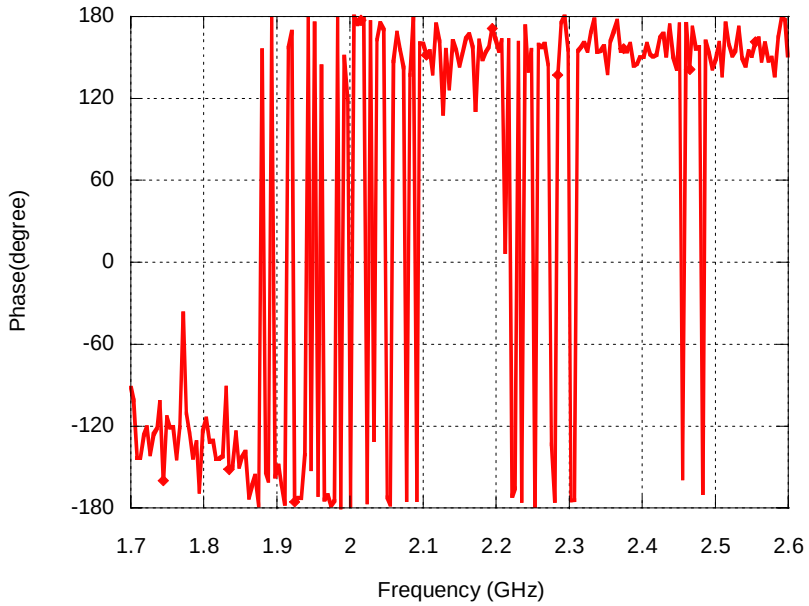

Fig. 16 – Phase of the average reflection coefficient of the second calibration performed in the second campaign.

Case # 3: Single slab of Plexiglass

After the previous two cases analyzed, which are necessary for the following tests, we have considered a single plexiglass slab (ε_r= 2.0). In Figures 17(a) and 17(b), it is possible to compare the results obtained in the two campaigns for this case (after the subtraction of the background contribution).

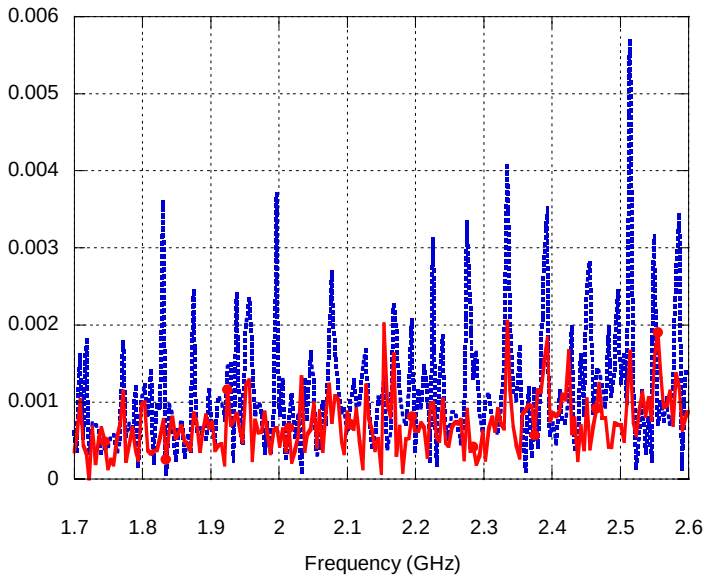

(a)

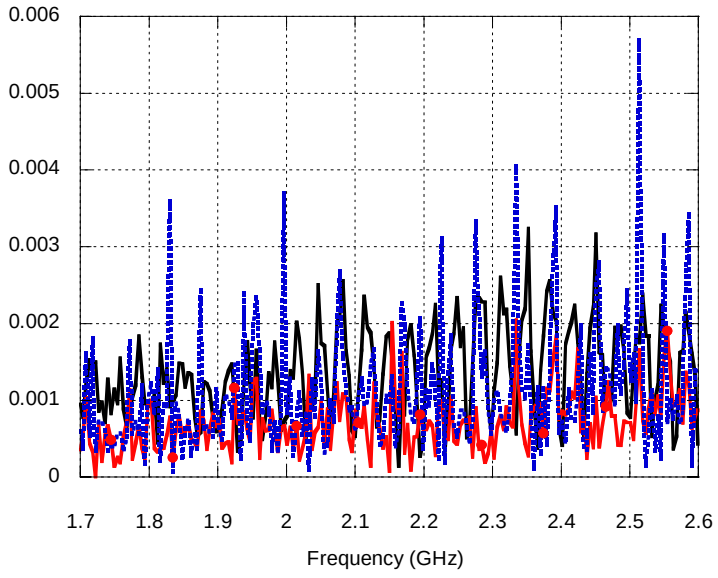

(b)

Fig. 17 – Comparison between the average of the reflection coefficient of the first (continuous red line with dots) and second (dashed blue line) calibration of the second campaign; (b) comparison between first (black line) and second (red and blue) campaign.

As said before, we have to normalize these data with respect to the PEC case. More in detail, we have adopted the following formula to normalize the reflection coefficient for each frequency f_i within our range:

$$\Gamma_{norm}(f_i) = \frac{\Gamma_{plex.}(f_i)}{\Gamma_{PEC}(f_i)}$$

In Fig. 18, it is possible to see the differences between the magnitudes of the computed reflection coefficient and the measured one. In Fig. 19, the comparison between the two resulting phases is reported.

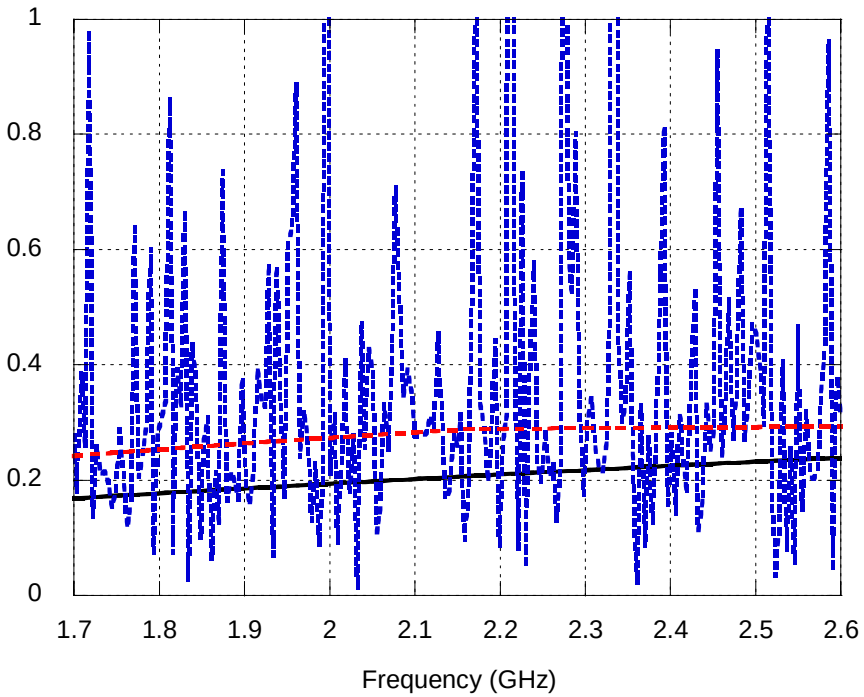

Fig. 18 – Comparison between the magnitudes of the normalized reflection coefficient: solver (black), normalized measurements (dashed blue), smooth version of measured data (dashed red).

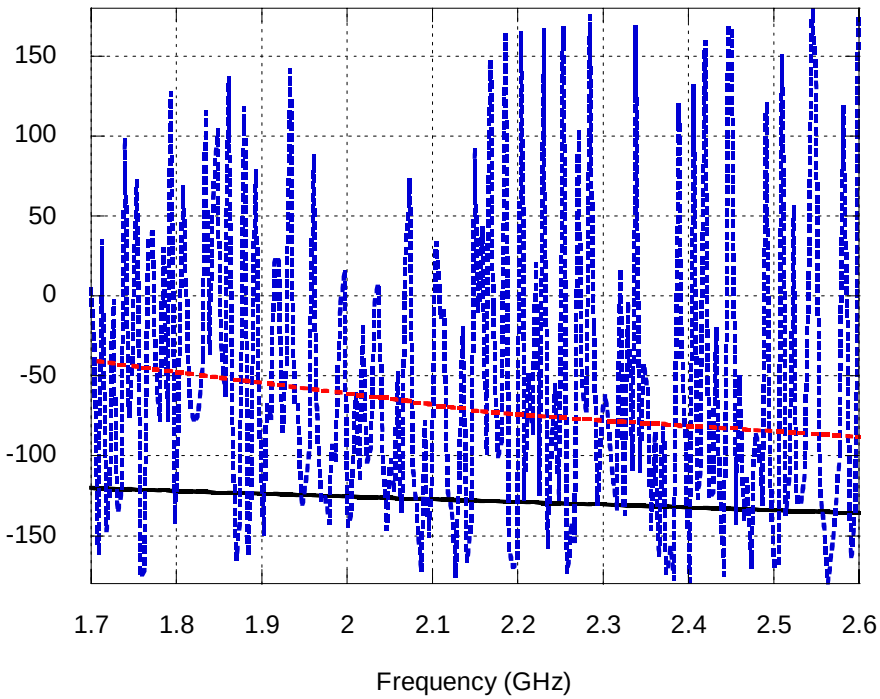

Fig. 19 – Comparison between the phases of the normalized reflection coefficient: solver (black), normalized measurements (dashed blue), smooth version of measured data (dashed red).

Case #4: Single alumina slab

In this case, we have analyzed a single slab of alumina (ε_r= 8.5). Figs 20(a) and 20(b) show the comparison between the average results obtained in the two campaigns for this case (after the subtraction of the background).

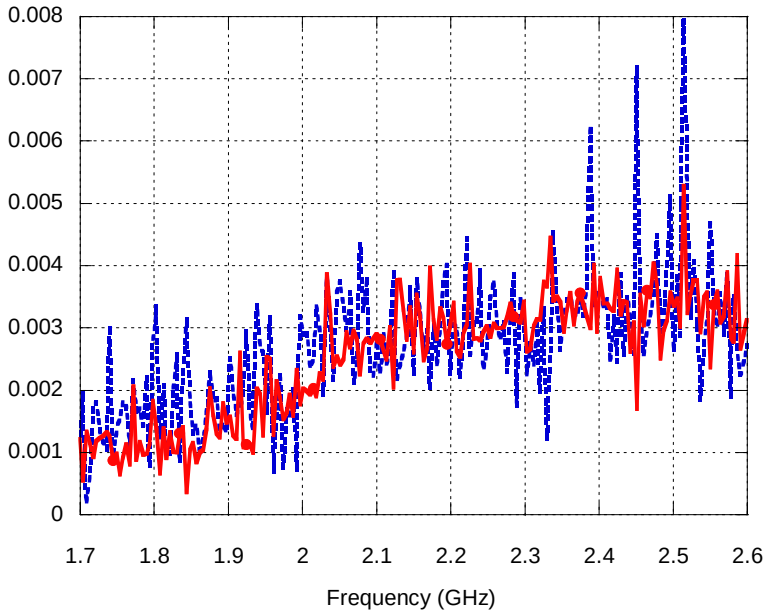

(a)

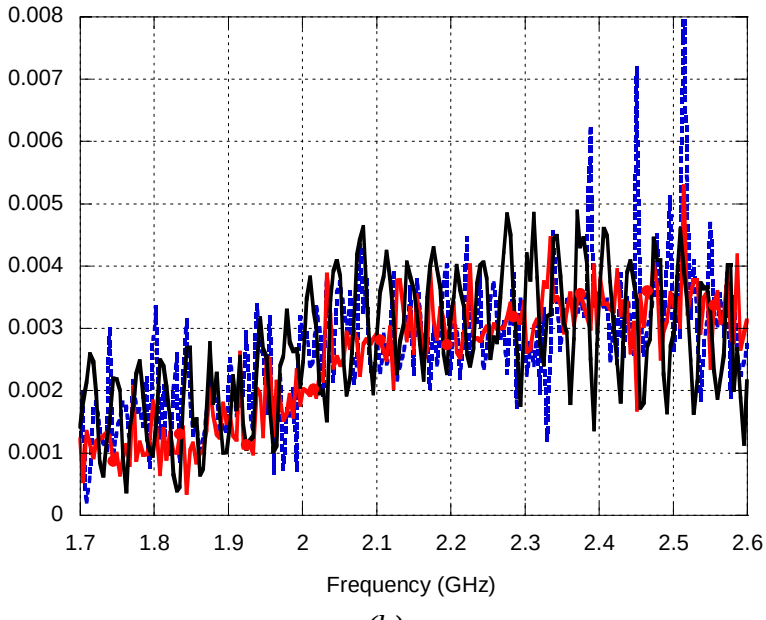

(b)

Fig. 20 – Comparison between the average magnitude of the reflection coefficient of the first (continuous red line with dots) and second (dashed blue line) calibration of the second campaign; (b) comparison between first (black line) and second (red and blue) campaign.

In Fig. 21, it is possible to compare the magnitude of the computed reflection coefficient with the measured one. The difference between the phases is shown in Fig. 22.

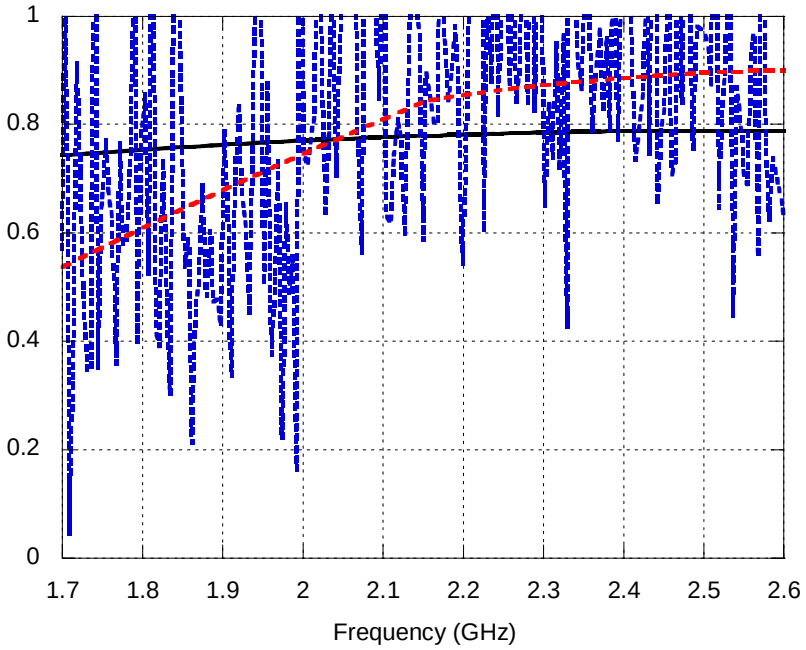

Fig. 21 – Comparison between the magnitude of the normalized reflection coefficient: solver (black line), normalized measurements (dashed blue line), smooth version of measured data(dashed red line).

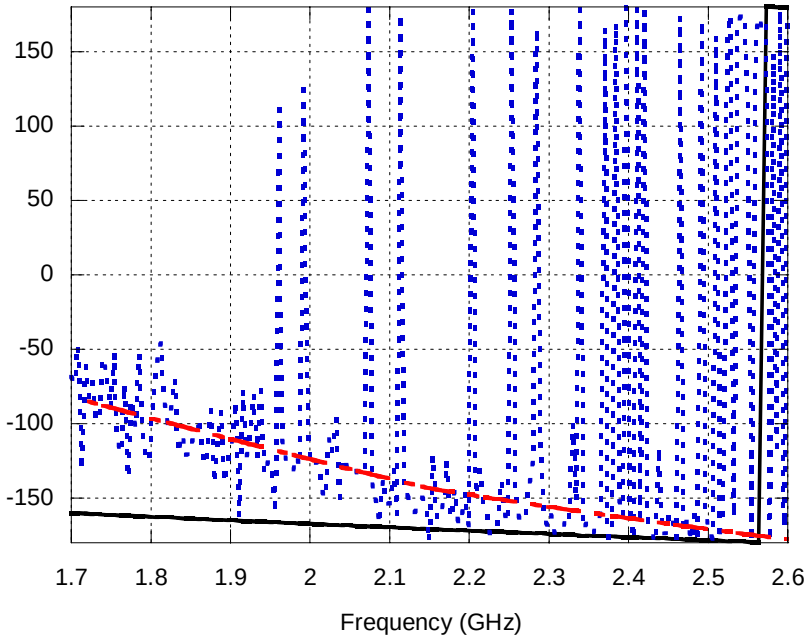

Fig. 22 – Comparison between the phase of the normalized reflection coefficient: solver (black line), normalized measurements (dashed blue line), smooth version of measured data (dashed red line).

Case #5: Alumina-Plexiglass-Alumina

The last case analyzed is a three-layer medium composed by a slab of plexiglass between two slabs of alumina. Each slab is thick one centimeter. In Fig 23 it is possible to compare the results obtained in the second campaign for this case (after the subtraction of the background).

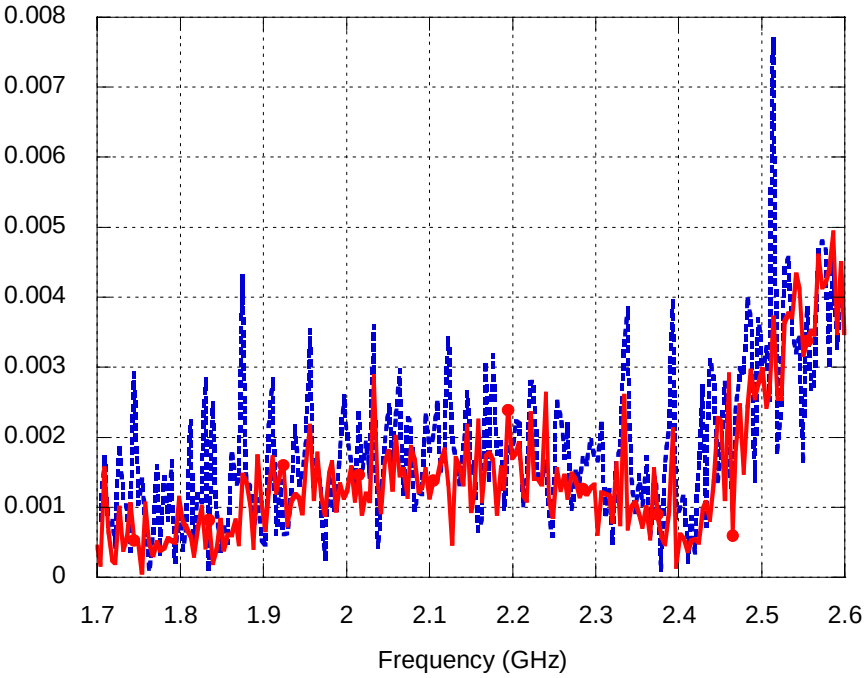

Fig. 23 – Comparison between the average magnitude of the reflection coefficient of the first (continuous red line with dots) and second (dashed blue line) calibration.

As in the previous case, it is reported the behavior of the magnitude of the computed reflection coefficient together with the measured one (Fig. 24). The comparison between the phases is shown in Fig. 25.

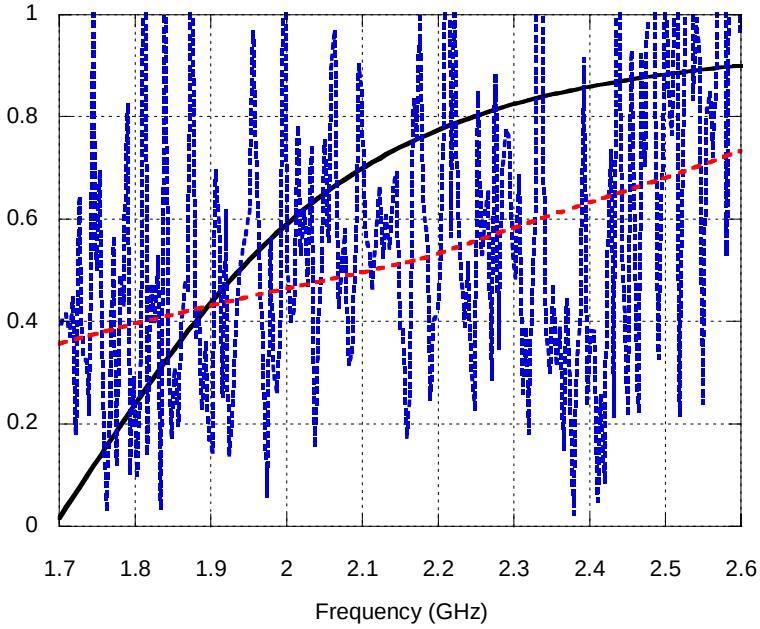

Fig. 24 – Comparison between the magnitude of the normalized reflection coefficient: solver (black), normalized measurements (dashed blue), smooth version of measured data(dashed red).

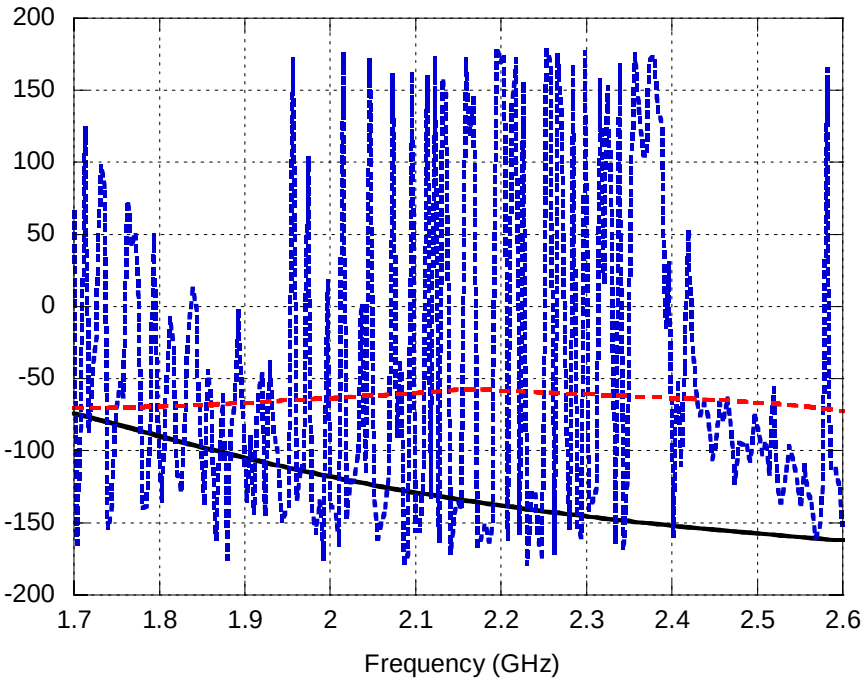

Fig. 25 – Comparison between the phase of the normalized reflection coefficient: solver (black line), normalized measurements (dashed blue line), smooth version of measured data(dashed red line).

Conclusion

The results obtained by using the solver completely agree with those of other commercial codes (HFSS and Designer). This fact proves the reliability of our software in the ideal case of a plane wave impinging with normal incidence to the interface between infinite layered media. Another interesting point we can highlight is the good agreement between the measurements obtained in the two different campaigns. If we consider the noise contribution, the almost complete accordance of the two data sets gives us a clear evidence that the measurements have been performed correctly.

However, the differences between the simulated and measured data are still difficult to be interpreted and the reasons for this are mainly two. First, the hypotheses upon which the solver is based are not verified. As far as plane-wave probing is concerned, we have tried to be as close as possible to the ideal case by using the far-field produced by an horn antenna to illuminate the investigated object. However, the HPBW is quite broad and then, the more we search for a simil-plane wave front, the less power impinges on the object. A second critic aspects regards the normalization of the measured quantities. The measurements of the field backscattered from the PEC slab does not solve completely the problems related to our non perfect knowledge of both the antenna gain and the distance between the object and the source. In fact, we have normalized all the data to the reflection coefficient obtained in the case of a PEC sample because we expected the maximum level of reflected power in this case. However, in same frequency range, the reflected power for the PEC slab is almost equal to that one reflected by a dielectric slab (cfr. Fig.7 and Fig.15) and this seems a quite strange result. Therefore, the finiteness of the slabs under test, very far from the ideal condition of infinite extension of the medium, is perhaps the aspect which affects more the results.

In spite of these limitations, it is possible to notice a quite good agreement at least for the plexiglass case and a similar trend of the responses in the case of the single slab of allumina.

References

[1] Salerno E., Genovesi S., Monorchio A., Manara G., “Edge-preserving permittivity range profile reconstruction by a genetic algorithm”, ISTI-CNR, Pisa, Italy, Technical report 2004-TR-66, December 2004.

[2] Bozzi E., Chimenti M., Genovesi S., Salerno E., Zucchelli A., “Equipment and procedures for microwave nondestructive evaluation of lapideous materials”, in P. Hazdra and M. Mazanek, eds., *Proc. 13th Conf. on Microwave Techn. - COMITE 2005*, Prague, Czech Republic, 26-28 September 2005, pp. 68-71.

[3] Genovesi S., Salerno E., Monorchio A., Manara G., “A permittivity range profile reconstruction technique for multilayered structures by a line process-augmented genetic algorithm”, *Proc. 2005 IEEE AP-S International Symposium*, Washington DC, 5-8 July 2005.

[4] Ansoft Corporation: www.ansoft.com/products/hf/hfss and www.ansoft.com/ansoftdesigner.

[5] CST – Computer Simulation Technology: http://www.cst.com.